Synthesis, crystal structure, microstructure and mechanical properties of $(Ti_{1-x}Zr_x)_3SiC_2$ MAX phase solid solutions

Qu, Lianshi; Bei, Guoping; Stelzer, Bastian; Rueß, Holger; Schneider, Jochen M.; Cao, Dianxue; van der Zwaag, Sybrand; Sloof, Willem G.

DOI
10.1016/j.ceramint.2018.10.030

Publication date
2019

Document Version
Final published version

Published in
Ceramics International

Ceramics International 45 (2019) 1400–1408

Contents lists available at ScienceDirect

Ceramics International

journal homepage: www.elsevier.com/locate/ceramint

Synthesis, crystal structure, microstructure and mechanical properties of $(Ti_{1-x}Zr_x)_3SiC_2$ MAX phase solid solutions

Lianshi Qu[a,b,*], Guoping Bei[b], Bastian Stelzer[c], Holger Rueß[c], Jochen M. Schneider[c], Dianxue Cao[a], Sybrand van der Zwaag[d], Willem G. Sloof[b]

[a] College of Materials Science and Chemical Engineering, Harbin Engineering University, Harbin 15001, China
[b] Department of Materials Science and Engineering, Delft University of Technology, Delft Mekelweg 2, 2628 CD Delft, the Netherlands
[c] Materials Chemistry, RWTH Aachen University, Kopernikusstrasse 10, 52074 Aachen, Germany
[d] Novel Aerospace Materials group, Faculty Aerospace Engineering, Kluyverweg 1, 2629 HS Delft, the Netherlands

ARTICLE INFO

Keywords:
MAX phases
$(Ti_{1-x}Zr_x)_3SiC_2$
Solid solution
Crystal structure
Mechanical properties

ABSTRACT

Almost pure $(Ti_{1-x}Zr_x)_3SiC_2$ MAX phase solid solutions with x ranging up to 0.17 were synthesized at temperatures in the range of 1450–1750 °C with reactive Spark Plasma Sintering (SPS). The zirconium partially replaces the M-element titanium of the Ti_3SiC_2 MAX phase up to x equals 0.17. The lattice parameters of the hexagonal $(Ti_{1-x}Zr_x)_3SiC_2$ MAX phase are determined with X-ray diffraction using Rietveld refinement and show an anisotropic lattice expansion upon Zr insertion into Ti_3SiC_2. This observation is in very good agreement with density functional theory calculations where the deviation between the measured and calculated lattice parameter is less than 1%. The predicted elastic modulus reduction is only 4%. This behavior can be rationalized by considering the electronic structure, where only minute changes are observable as Zr is incorporated into Ti_3SiC_2. The measured nanohardness of the synthesized $(Ti_{1-x}Zr_x)_3SiC_2$ MAX phase increases from 12.7 ± 1 GPa for Ti_3SiC_2 to 16.3 ± 1.1 GPa when x is raised from 0 to 0.17 due to an increasing amount of accompanying $Ti_{1-y}Zr_yC$. The elastic moduli of $(Ti_{1-x}Zr_x)_3SiC_2$ solid solutions measured by an ultrasonic pulse-echo method (325–354 GPa) are in good agreement with the predicted elastic moduli (357–342 GPa).

1. Introduction

MAX phases are a family of ternary nitrides and carbides, with the general formula $M_{n+1}AX_n$ (n = 1–3), where M is an early transition metal, A is an A group element, and X is either carbon or nitrogen [1–3]. MAX phases have a hexagonal crystal lattice (space group *P63/mmc*) with an edge-sharing $[M_6X]$ octahedral interleaved by an A layer. In this nanolayered structure, the M atoms and X atoms are connected by strong covalent bonds, while the M atoms and A atoms are connected by weaker metallic bonds [1–3]. Because of their unique structure, MAX phases exhibit a combination of merits of both metals and ceramics, such as: good thermal and electrical conductivity, relatively low hardness, damage tolerance, good oxidation resistance and resistance to chemical attack as well as excellent machinability [2,3]. Some MAX phases, like Cr_2AlC [4], Ti_2AlC [5] and Ti_2SnC [6], also show self-healing behavior upon exposure to air at high temperatures. Cracks are then healed by filling the crack opening with well-adhering M-oxides and A-oxides [7]. This makes these MAX phases attractive materials for high temperature structural components and electrical contact materials [2,3].

Both experimental and computational studies suggest that many solid solution permutations and combinations in MAX phases are possible by substitution of the base element with other elements of the same group at the M-site [8–13], the A-site [14–23] and/or the X-site [24,25]. This opens opportunities to manipulate and tune properties of MAX phase materials. For example, a solid solution hardening effect has been observed in $Ti_3(Al_{0.75}Si_{0.25})C_2$ [18] and $Ti_2Al(C_{0.5}N_{0.5})$ [24]. The oxidation kinetics and crack healing behavior can be modified by partial substitution of Al by Sn in the Ti-Al-C MAX system [19,26]. More recently, Zr contained MAX phases (Zr_2AlC [13]) and related solid solutions $(Nb_{1-x}Zr_x)_4AlC_3$ [28], Zr-Ti-Al-C [13], and $(Ti_{1-x}Zr_x)_3(SiAl)C_2$ [27] have been synthesized. For example, $(Nb_{0.85}, Zr_{0.15})_4AlC_3$ MAX phase can maintain its flexural strength of 311 ± 57 MPa up to temperatures of 1450 °C [28] and $(Ti_{1-x}Zr_x)_3(SiAl)C_2$ can retain high degrees of stiffness and strength up to 1200 °C, which is 150 °C higher than those for $Ti_3(Si,Al)C_2$ [27]. This suggests that substitution of a fourth element at the M lattice position of a MAX phase can improve its high temperature strength and stiffness [27,28].

* Corresponding author.
E-mail address: qulianshi2006@163.com (L. Qu).

https://doi.org/10.1016/j.ceramint.2018.10.030
Received 24 August 2018; Received in revised form 2 October 2018; Accepted 3 October 2018
Available online 10 October 2018

Ti_3SiC_2 is a representative member of 312 MAX phases [1], which attracted a lot of attention when Barsoum et al. synthesized highly pure bulk Ti_3SiC_2 ceramic by reactive Hot Isostatic Pressing (HIP) and reported its salient properties [29]. Since then, the microstructure and properties of Ti_3SiC_2 were investigated in great detail [30]. To synthesize Ti_3SiC_2 as a bulk ceramic, various methods were used, such as: HIP, Hot Pressing (HP) and Spark Plasma Sintering (SPS) or Pulse Discharge Sintering (PDS). Different powder mixture compositions were explored, such as: Ti/SiC/C, Ti/Si/C, Ti/SiC/TiC, TiH_2/Si/TiC and Ti/Si/TiC [30], and the optimal synthesis conditions for almost pure Ti_3SiC_2 are now well established. However, the synthesis of Ti_3SiC_2 based solid solutions, where solely the M-site element is substituted, has not been reported yet. Hence, this work focuses on the synthesis of Ti_3SiC_2 based solid solutions by substitution at the M-site. Preliminary ab initio calculations based on Density Functional Theory (DFT) suggested that Zr can be dissolved over a wide composition range. The partial substitution of Ti by Zr is studied in $(Ti_{1-x}Zr_x)_3SiC_2$ MAX phase with x varied between 0 and 0.17. This material was prepared by SPS using Ti/Zr/Si/TiC powder mixtures and temperatures in the range of 1450–1750 °C. X-ray diffraction analysis and DFT calculations were used to determine the effect of Zr solid solution on the crystal lattice parameters. The composition and microstructure of the as synthesized $(Ti_{1-x}Zr_x)_3SiC_2$ MAX phase was investigated and their mechanical properties, such as elastic modulus and hardness, as a function of the Zr concentration were determined by nanoindentation and microindentation as well as ultrasonic pulse-echo method as a function of the Zr concentration.

2. Experimental details

Powders of Ti (100 µm, 99.5% purity, TLS Technik GmbH & Co), Zr (45 µm, 99.2% purity, TLS Technik GmbH & Co), Si (45 µm, 99.99% purity, TLS Technik GmbH & Co) and TiC (10 µm, 99% purity, CHEMPUR, Feinchemikalien und Forschungsbedarf GmbH) were used as starting materials. Powder mixtures of different compositions (see Table 1) were prepared in a glovebox (M. Braun Inertgas Systeme GmbH, Germany) purged with Ar (5 N purity, Linde), while the oxygen level was below 0.5 ppm and the moisture level below 1.7 ppm H_2O. Then, these powder mixtures were blended for 4 h with a Turbula mixer (Type T2C, Willy A. Bachofen AG, Basel, Switzerland) using a mixture of Al_2O_3 balls with a ratio of 1: 5 of 10 and 5 mm diameter balls, respectively.

The powder mixture was put into a graphite die with an inner diameter of 20 mm and covered from both sides with graphite punches (ISO-68, Toyo Tanso, Japan). Graphite foils (Papyrex Mersen, France) were used to prevent possible reaction between the powder and the graphite die and punches. In addition, these graphite foils were sprayed with BN (Henze Boron Nitride Products AG, Lauben, Germany) on both sides for easy removal of the sample. Subsequently, the powder mixture in the graphite die and punches assembly was SPSed in a furnace (HP D 25 SD, FCT system GmbH, Germany) at temperatures in the range of 1450–1750 °C for 1 h while applying a pressure of 50 MPa applied form the beginning of sintering cycle and flushing the furnace with pure Ar (5 N purity, Linde, The Netherlands). A heating and cooling rate of about 50 °C/min was applied. The temperature was monitored using an axial pyrometer. The electric current was applied following 15/5 (on/off 3 ms) pulse sequence. Finally, after releasing the pressure from the material, it was cooled from the sintering temperature to room temperature. Key process parameter settings for the synthesis of $(Ti_{1-x}Zr_x)_3SiC_2$ MAX phase solid solutions are listed in Table 1.

Table 1
Composition of the powder mixtures to synthesize $(Ti_{1-x}Zr_x)_3SiC_2$ with SPS at 50 MPa for 1 h in pure Argon at the indicated sintering temperatures.

Compound	Powder mixtures (molar ratios)	Sintering temperature (°C)
$(Ti_{1-x}Zr_x)_3SiC_2$	1.0Ti-1.0Si-1.9TiC	1450
	0.9Ti-0.1Zr-1.0Si-1.9TiC	1450–1500
	0.8Ti-0.2Zr-1.0Si-1.9TiC	1450–1500
	0.7Ti-0.3Zr-1.0Si-1.9TiC	1450–1600
	0.6Ti-0.4Zr-1.0Si-1.9TiC	1450–1700
	0.5Ti-0.5Zr-1.0Si-1.9TiC	1450–1750
Zr_3SiC_2	1.0Zr-1.0Si-1.9ZrC	1700
	3.0Zr-1.0Si-2.0C	1450–1700
	3.0ZrH_2-1.0Si-2.0C	1500–1650
	3.0Zr-1.0Si-2.0C-0.1Fe	1450–1500

After SPS, the surfaces of the samples were ground with SiC emery paper staring with 240 grit and finishing with 4000 grit. Finally, the surfaces were polished with 1 µm diamond grains suspension on a soft cloth. The density of the synthesized MAX phase bulk was measured by the Archimedes method using an analytical balance (Mettler Toledo, AG-204, Switzerland) according to ASTM B 3962–15 [31].

The phase composition was determined with X-Ray Diffraction (XRD) analysis using a Bruker D8 Advance diffractometer operated with Cu Kα radiation. Diffractograms were recorded in the 2θ range of 8–80° with a step size of 0.02° and a counting time per step of 1 s. These diffractograms were evaluated using the Bruker Diffrac EVA software (Version 3). The lattice parameters of synthesized solid solutions were obtained with Rietveld refinement using MAUD software [32]. A LaB_6 powder was applied as a reference material to correct the diffraction angle for instrumental errors [33]. For the Rietveld refinement, datafiles of Ti_3SiC_2 (hexagonal, $P63/mmc$, $a = 3.0665$ Å and $c = 17.6710$ Å) and TiC (cubic, Fm-3m, $a = 4.3176$ Å) were applied. The specific parameters refined in the MAUD software including the background subtraction, line broadening (microstructure), position of the M element (i.e. Ti and Zr), specimen displacement, and lattice parameters etc.. After a reliable refinement, the weighted reliability factors were in the 6.9–9.8% range.

The microstructure was observed with Scanning Electron Microscopy (SEM) using a JSM 6500 F (Jeol, Japan) equipped with an Energy Dispersive Spectrometer (EDS) for X-ray microanalysis (XMA). This EDS is an Ultra Dry detector (30 mm^2) operated with Noran System Seven software package (ThermoFisher, USA) for data acquisition and analysis. The volume fraction of the different phases as well as the porosity was determined by image analysis by using ImageJ software (version 1.49 V). To this end, a surface area of at least 4 × 4 mm of the sintered sample was recorded with SEM.

The chemical composition of synthesized $(Ti_{1-x}Zr_x)_3SiC_2$ solid solutions was determined with Electron Probe X-ray Microanalysis (EPMA) using Wavelength Dispersive Spectrometry (WDS). For this purpose, A Jeol JXA 8900R superprobe operated with focused electron beam energy of 15 keV and a current of 50 nA was used. Prior to each measurement the surface of the specimen was decontaminated using an air-jet for 30 s. The composition at each analysis location was determined using the X-ray intensities (C Kα, Si Kα, Ti Kα, and Zr Kα of the constituent elements after background correction relative to the corresponding intensities of reference materials, viz. Fe_3C (cementite) [34] or C and pure elements for Si, Ti, and Zr, respectively. The obtained intensity ratios were processed with a matrix correction program CITZAF to compute the composition.

Both the microhardness and nanohardness were determined by Vickers indentation tests and nanoindentation tests, respectively. The Vickers microhardness was measured with a Zwick/Z2.5 hardness tester (Ulm, Germany) in a load range of 0.5–100 N and at a constant contact time of 10 s. Nanoindentation measurements were performed with a Hysitron TI-900 Triboindenter (Bruker, Germany) equipped with a diamond Berkovich indenter. Before performing the nanoindentation measurements on the MAX phase samples, the tip area function was calibrated by indenting fused silica with a known elastic or Young's modulus of 72 GPa [20]. In order to investigate the hardness variation with varying displacements, five different loads (1, 2, 3, 6, 10 mN) were applied. For every single load, 36 indentations were performed at each sample. The load-displacement curves were recorded and the hardness

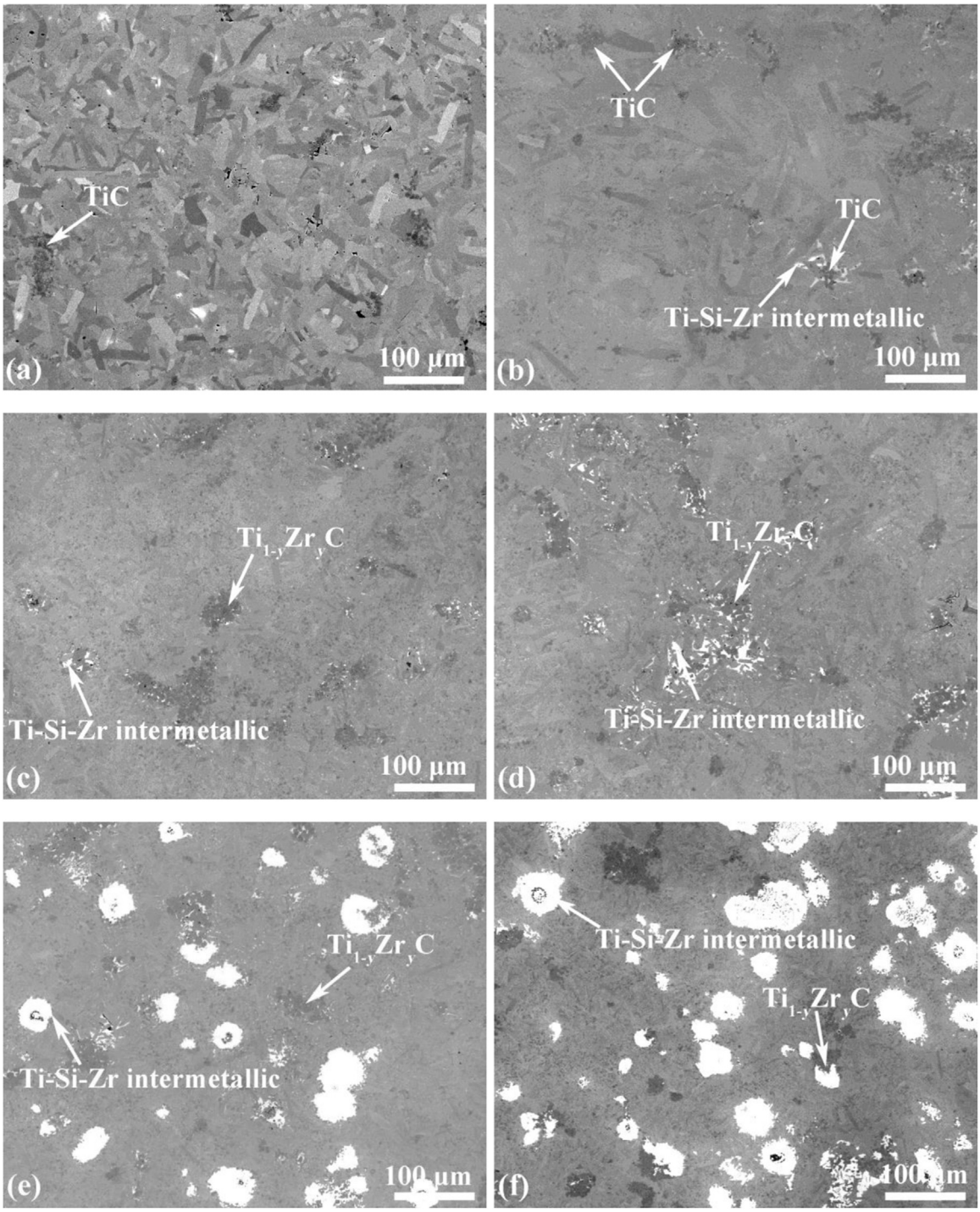

Fig. 1. SEM backscattered electron images of $Ti_{3-x}Zr_xSiC_2$ MAX phase synthesized with SPS at 1450 °C for 1 h with a pressure of 50 MPa from powder mixtures with different Zr content; composition in mol fraction: (a) 1.0Ti-1.0Si-1.9TiC, (b) 0.9Ti-0.1Zr-1.0Si-1.9TiC, (c) 0.8Ti-0.2Zr-1.0Si-1.9TiC (d) 0.7Ti-0.3Zr-1.0Si-1.9TiC (e) 0.6Ti-0.4Zr-1.0Si-1.9TiC, and (f) 0.5Ti-0.5Zr-1.0Si-1.9TiC.

and elastic modulus was determined from the unloading curve employing the Oliver and Pharr method [35,36], albeit. To eliminate the indentation size effect on the hardness values of the MAX phase the mathematical function of the Nix and Gao model [37] was adopted, albeit this function may not be valid (cf [38].) for the small indentation depths in this work. Thus, a limit hardness value was determined that is considered as a hardness value of MAX phase [20].

Furthermore, the elastic modulus of synthesized MAX phase solid solution was also determined with a pulse-echo method using an ultrasonic testing device (Model USIP 11, Krauthrämer, Germany). As a transmitting and receiving transducer of the sound waves, a MB4S-N probe was used producing ultrasounds of 4 MHz. For the interface couplant between transducer and sample, oil (Panametrics, Waltham, USA) was applied. From the measured longitudinal sound velocity c_l through the material the elastic modulus was calculated using the following relation applicable for isotropic materials [39]:

$$E = \frac{(1+\nu)(1-2\nu)}{(1-\nu)}\rho c_l^2 \quad (1)$$

where ν is Poisson's ratio and ρ is the density of the prepared material.

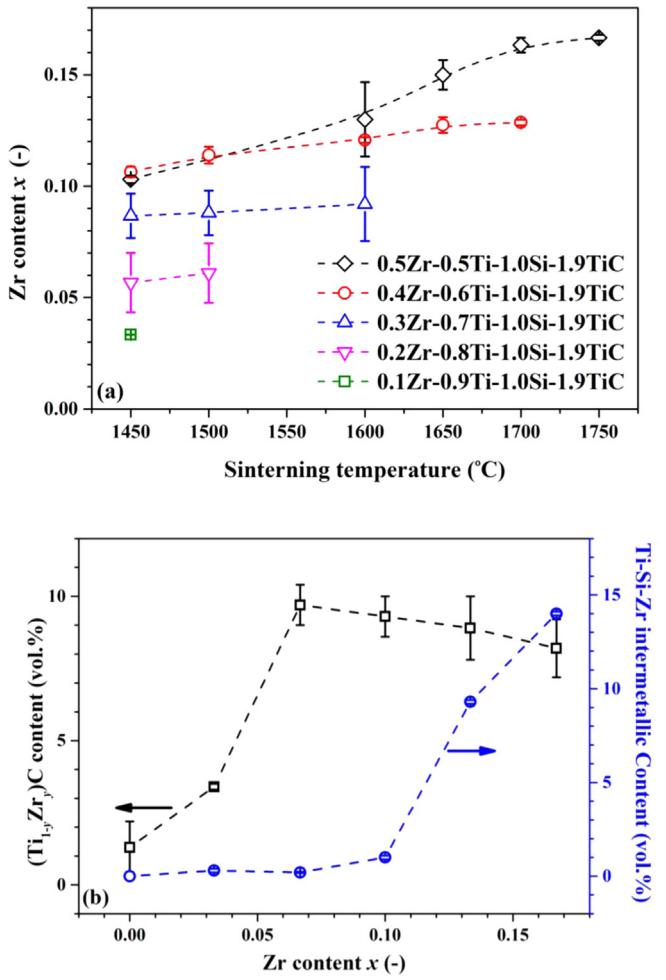

Fig. 2. (a) Zr content (x) of $(Ti_{1-x}Zr_x)_3SiC_2$MAX phase versus the sintering temperature during SPS. The molar fraction of the constituents of the starting powder mixtures is indicated in the legend. (b) The volume fraction of $(Ti_{1-y}Zr_y)C$ phase and Ti-Si-Zr intermetallic in the samples, sintered at 1450 °C for 1 h under a pressure of 50 MPa by SPS, as a function of the Zr content x in the powder mixture.

Here a value of 0.2 for the Poisson's ratio was adopted [1]. Each data point for the elastic modulus comprises measurements of 5 samples per composition.

3. DFT calculations

Ab initio calculations are carried out using Density Functional Theory (DFT) [40] as implemented in the Vienna *Ab Initio* Simulation Package (VASP) [41,42] wherein projector augmented wave potentials [43] are employed. The generalized-gradient approximation, as introduced by Perdew, Burke and Ernzerhof [44], a convergence criterion for relaxation of 0.01 meV and Blöchl corrections for the total energy [45] cut-off of 500 eV are applied. Brillouin zone integration was carried out with a $7 \times 7 \times 5$ Monkhorst–Pack k-point mesh [46]. $2 \times 2 \times 1$ supercells with 48 atoms were utilized for the solid solution $(Ti_{1-x}Zr_x)_3SiC_2$ MAX phase with $x = 0$, 0.09, 0.17 and 0.25, where Ti atoms were substituted by Zr atoms. Full structural relaxation was performed for every configuration and the Birch–Murnaghan equation of state [47] was utilized to obtain the equilibrium volume and bulk moduli. Elastic modulus was obtained from bulk modulus data assuming a Poisson´s ratio of 0.2 [1].

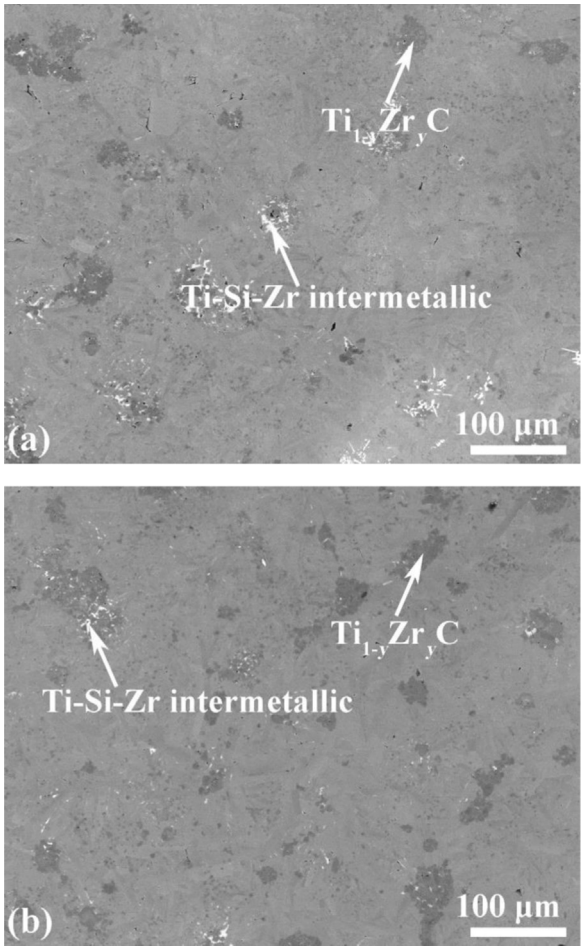

Fig. 3. SEM backscattered electron images of the material after sintering of a 0.7Ti-0.3Zr-1.0Si-1.9TiC powder mixture with SPS at: (a) 1500 °C and (b) 1600 °C.

4. Results and discussion

4.1. Synthesis of $(Ti_{1-x}Zr_x)_3SiC_2$ MAX phase solid solutions at 1450 °C

The microstructure of the synthesized $(Ti_{1-x}Zr_x)_3SiC_2$ MAX phase with various Zr content prepared at 1450 °C is shown in Fig. 1. The Zr free synthesized material consists of mainly Ti_3SiC_2 with typical elongated grains and 1.3 ± 0.9 vol% TiC; see Fig. 1(a). Almost all the Zr in the 0.9Ti-0.1Zr-1.0Si-1.9TiC powder mixture is dissolved in Ti_3SiC_2 after SPS; see Fig. 1(b). However, when the relative amount of Zr added to the powder mixture is increased above this level, not all the Zr is dissolved in Ti_3SiC_2. For example, after sintering of the 0.5Ti-0.5Zr-1.0Si-1.9TiC powder mixture only 60% of the Zr is dissolved in Ti_3SiC_2 (see Fig. 2(a)), which corresponds with x equal to 0.1 in $(Ti_{1-x}Zr_x)_3SiC_2$. The remainder of the Zr is dissolved in the second phase TiC and precipitated as Ti-Si-Zr intermetallic; see Figs. 1(c) to (f).

The Zr dissolved in TiC results in the formation of $(Ti_{1-y}Zr_y)C$ solid solution [13], and the amount dissolved increases with the relative amount of Zr added to the powder mixture. The volume fraction of $(Ti_{1-y}Zr_y)C$ phase in the final product amounts up to about 10 vol% when the mole fraction Zr added to the powder mixture is more than 5%; see Fig. 2(b).

Concerning the formation of the unwanted Ti-Si-Zr intermetallic phase, its volume fraction is less than 1.0 vol% when the mole fraction Zr added to the powder mixture is less than 10%; see Fig. 2(b). However, when the mole fraction Zr added to the powder mixture is 10.3% and 12.8%, the volume fraction of the Ti-Si-Zr intermetallic in the final

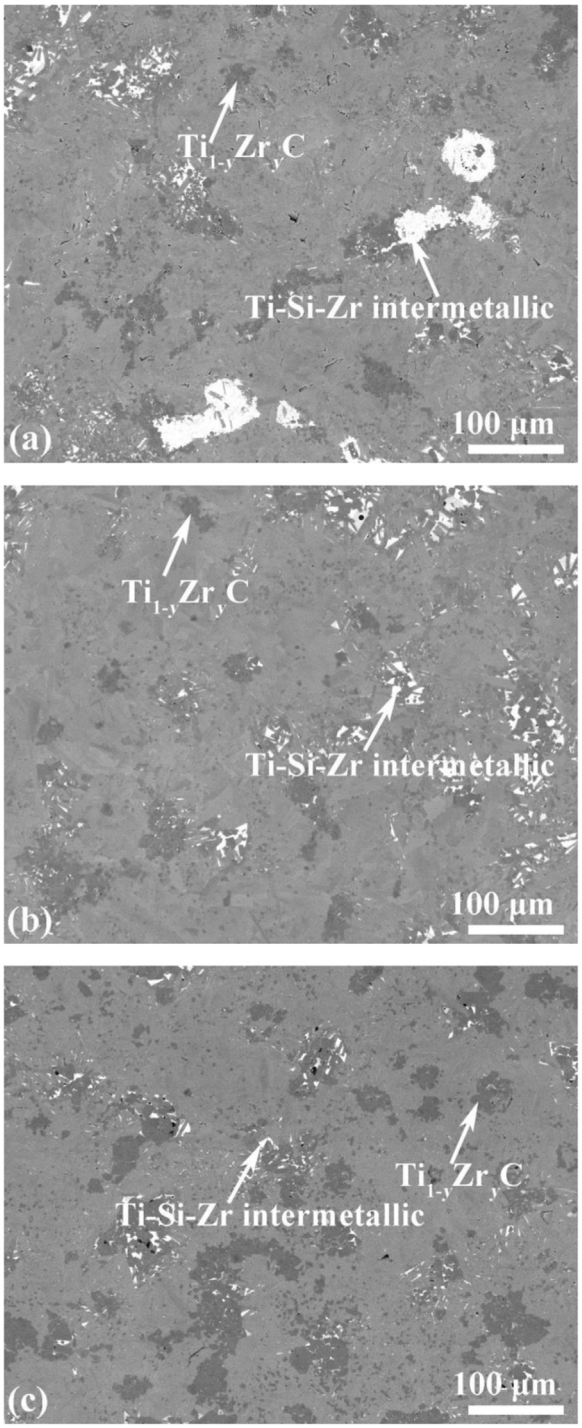

Fig. 4. SEM backscattered electron images of the material after sintering 0.5Ti-0.5Zr-1.0Si-1.9TiC powder mixture with SPS at: (a) 1600 °C, (b)1650 °C, and (c) 1750 °C.

product is 9.3 ± 0.1 and 14.0 ± 0.1 vol%, respectively.

4.2. Effect of sintering temperature on the phase composition

It is expected that increasing the sintering temperature will favor the dissolution of an alloying element; see e.g [48]. Thus, to improve the dissolution of Zr in Ti_3SiC_2, higher sintering temperatures were applied. For example, the microstructure of the material after SPS of a 0.7Ti-0.3Zr-1.0Si-1.9TiC powder mixture at temperatures higher than 1450 °C are shown in Fig. 3. Increasing the sintering temperature to 1500 °C the amount of Zr in solid solution, i.e., x value in the $(Ti_{1-x}Zr_x)_3SiC_2$, increased from 0.082 ± 0.01–0.088 ± 0.01; see Fig. 2(a). When increasing the sintering temperature to 1600 °C the amount of Zr in solid solution is up to 0.09 ± 0.02, revealing that almost all the Zr in the powder mixture is dissolved in Ti_3SiC_2.

Further increase of the amount of Zr in the powder mixture may require even higher sintering temperatures to promote dissolution into Ti_3SiC_2. For example, after sintering a 0.5Ti-0.5Zr-1.0Si-1.9TiC powder mixture at 1600, 1650 and 1750 °C, the value of x in $(Ti_{1-x}Zr_x)_3SiC_2$ increased to 0.13 ± 0.02, 0.150 ± 0.006 and 0.167 ± 0.001 respectively; see Fig. 2(a). The Zr content in the $(Ti_{1-x}Zr_x)_3SiC_2$ are more homogenous when synthesized at higher temperatures.

When increasing the sintering temperature of the 0.5Ti-0.5Zr-1.0Si-1.9TiC powder mixture from 1600° to 1750°C, the volume fraction of $(Ti_{1-y}Zr_y)C$ increased from 17.2 ± 0.1–28.1 ± 2.2 vol%, while the volume fraction of the Ti-Si-Zr intermetallic phase decreased from 4.0 ± 0.6–1.5 ± 0.2 vol%, respectively; see Fig. 4. Thus, a higher sintering temperature is required to fully dissolve Zr into Ti_3SiC_2 for the powder mixtures with a relatively high Zr content. However, a large amount of the $(Ti_{1-y}Zr_y)C$ phase will be present in the final product due to either the loss of Si [3,30] or decomposition of $(Ti_{1-x}Zr_x)_3SiC_2$ at higher temperatures. Hence, there is a practical limit for the amount of Zr that can be dissolved into Ti_3SiC_2. For the sintering conditions applied here, x equal to 0.17 seems to be the maximum. Adding more Zr to the powder mixture only results in more second phases.

The conditions to sinter different powder mixtures to form $(Ti_{1-x}Zr_x)_3SiC_2$, where almost all Zr is fully dissolved, is listed in Table 2. The phase composition of the $(Ti_{1-x}Zr_x)_3SiC_2$ and $(Ti_{1-y}Zr_y)C$ solid solutions determined by EMPA are also listed in Table 2. The Zr content in the $(Ti_{1-x}Zr_x)_3SiC_2$ phase is slightly smaller than is expected from the amount of Zr in the powder mixture. This is due to partial dissolution of Zr in the $(Ti_{1-y}Zr_y)C$ phase and the formation of Ti-Si-Zr intermetallics at the grain boundaries.

4.3. Synthesis of Zr_3SiC_2

According to our DFT calculations (where the corresponding elements are employed as reactants) Zr_3SiC_2, as an end member of $(Ti_{1-x}Zr_x)_3SiC_2$ (i.e., $x = 1$) may be exist. In an attempt to prepare Zr_3SiC_2, different powder mixtures were sintered at temperatures ranging from 1450 up to 1700 °C; see Table 1. However, only binary phases such as ZrC, Zr-Si intermetallics were detected with XRD and XMA. For example, the XRD analysis of 3.0Zr-1.0Si-2.0 C powder mixture SPSed at 1450 °C for 1 h with a pressure of 50 MPa shows that only ZrC, ZrSi, $ZrSi_2$ and Zr_5Si_3 were formed. These reaction products are in agreement with the results of ternary phase equilibria investigations of the Zr-Si-C system at 1200 °C [49] and 1300 °C [50] and 1600 °C [51] where also no Zr_3SiC_2 phase analogous to Ti_3SiC_2 was detected. Furthermore, inspired by recent work on the synthesis of MAX phase in the Zr-Al-C system [13], ZrH_2 was used in the powder mixture and some iron was added as a catalyst. But also, this attempt failed.

4.4. Crystal structure of $(Ti_{1-x}Zr_x)_3SiC_2$ MAX phase solid solution

The diffractograms of the $(Ti_{1-x}Zr_x)_3SiC_2$ MAX phase solid solutions prepared at the optimized sintering temperatures with different Zr content (see Table 2) are shown in Fig. 5. In these diffractograms, only the $(Ti_{1-x}Zr_x)_3SiC_2$ MAX phase and the $(Ti_{1-y}Zr_y)C$ phase can be identified. With increasing Zr content of the starting powder mixture, the diffraction peaks of the $(Ti_{1-x}Zr_x)_3SiC_2$ and $(Ti_{1-y}Zr_y)C$ phase are shifted to smaller angles. Rietveld refinement of the XRD data allows determination of the lattice parameters as a function of Zr content of the solid solutions. Next, the lattice parameters of the $(Ti_{1-x}Zr_x)_3SiC_2$ and the $(Ti_{1-y}Zr_y)C$ phase determined from Rietveld refinement are given in Table 2 and plotted as a function of their Zr content; see Fig. 6. For comparison, the lattice parameters obtained from the ab initio

Table 2
Composition and lattice parameters of $(Ti_{1-x}Zr_x)_3SiC_2$ MAX phase and $Ti_{1-y}Zr_yC$ prepared by SPS with optimized sintering temperature including the densities. The composition was determined with EMPA, and the lattice parameters were from Rietveld refinement of X-ray diffractograms and DFT calculations.

Experimental results							DFT calculations	
Starting materials	Sintering Temp. (°C)	$(Ti_{1-x}Zr_x)_3SiC_2$		$Ti_{1-y}Zr_yC$		Density (g/cm^3)	$(Ti_{1-x}Zr_x)_3SiC_2$	
		x	Lattice parameters (Å)	y	Lattice parameter (Å)		x	Lattice parameters (Å)
1Ti-1Si-1.9TiC	1450	0	a = 3.067 c = 17.668	0	a = 4.319	4.46 ± 0.08	0	a = 3.071 c = 17.741
0.9Ti-0.1Zr-1Si-1.9TiC	1450	0.03	a = 3.074 c = 17.699	0.017	a = 4.326	4.595 ± 0.005	0.09	a = 3.097 c = 17.872
0.8Ti-0.2Zr-1Si-1.9TiC	1500	0.06	a = 3.084 c = 17.728	0.029	a = 4.333	4.67 ± 0.001	0.18	a = 3.123 c = 17.984
0.7Ti-0.3Zr-1Si-1.9TiC	1600	0.09	a = 3.092 c = 17.766	0.060	a = 4.344	4.71 ± 0.01	0.25	a = 3.149 c = 18.099
0.6Ti-0.4Zr-1Si-1.9TiC	1700	0.12	a = 3.106 c = 17.823	0.087	a = 4.360	4.80 ± 0.01		
0.5Ti-0.5Zr-1Si-1.9TiC	1750	0.17	a = 3.117 c = 17.864	0.109	a = 4.371	4.84 ± 0.07		

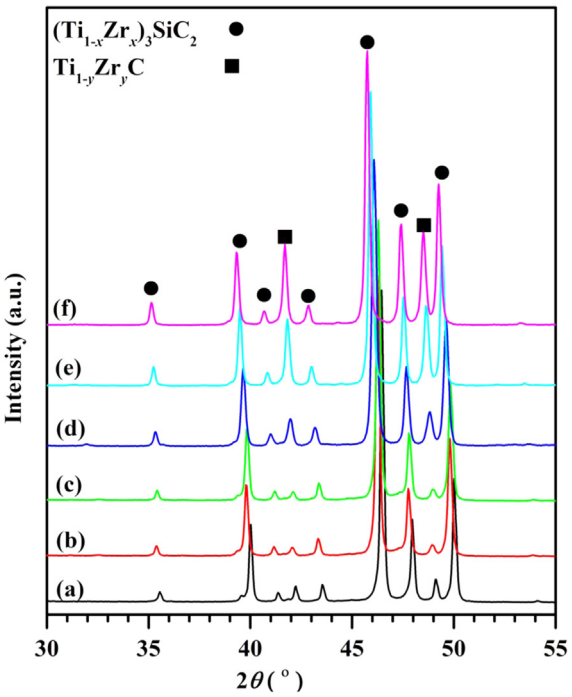

Fig. 5. XRD patterns of $(Ti_{1-x}Zr_x)_3SiC_2$ MAX phase solid solutions prepared with SPS from powder mixtures at optimized sintering temperature: (a) x = 0, (b) x = 0.03, (c) x = 0.06, (d) x = 0.09 (e) x = 0.12, and (f) x = 0.17.

calculations are also listed in Table 2 and plotted together with the experimental results in Fig. 6. As revealed in Fig. 6(a), substitution of Ti (atomic radius: 147 pm [52]) by Zr (atomic radius: 160 pm [52]) on the M site of the $(Ti_{1-x}Zr_x)_3SiC_2$ MAX phase results into an anisotropic lattice expansion. The relative expansion of the a axis is with 1.65% much larger than that of the c axis of the hexagonal crystal lattice (1.11%); viz.: a = 3.067 Å for x = 0 to a = 3.117 Å for x = 0.17 and c = 17.668 Å for x = 0 to c = 17.864 Å for x = 0.17, respectively. The lattice parameters of $(Ti_{1-x}Zr_x)_3SiC_2$ MAX phase solid solutions obtained from the ab initio calculations are in good agreement with the experimental results reported for $(Ti_{1-x}Zr_x)_3SiC_2$ solid solution with x up to 0.07 [27]; see Fig. 6. The observed and predicted increase of the lattice parameters a and c can be rationalized by considering the difference in metallic radii between Ti and Zr. This difference of the metallic radii is 9.4%, while the valence electron concentration is constant as Ti is substituted by Zr.

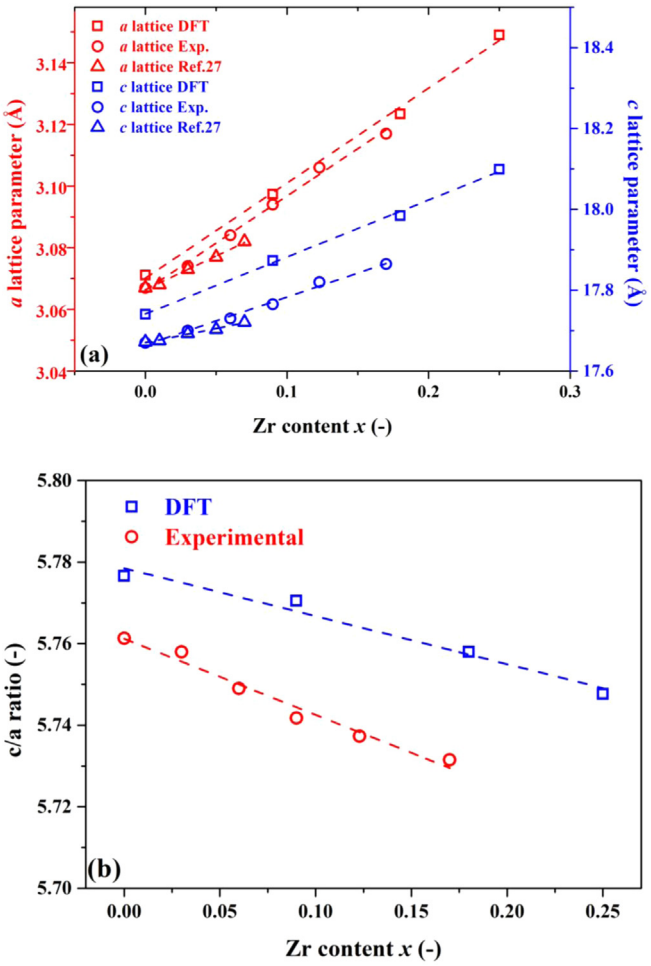

Fig. 6. Lattice parameters a and c of $(Ti_{1-x}Zr_x)_3SiC_2$MAX phase with hexagonal crystal lattice as a function of Zr content: (a) lattice parameters, (b) c/a ratio.

Next, a linear reduction of the c/a ratio with increasing Zr content in solid solution is observed for both the experimental results as well as the ab initio calculations; see Fig. 6(b). This behavior of the lattice parameters is consistent with the formation of an ideal solid solution following Vegard's law [53]. The M-site substitution induced lattice parameter changing corresponds with results of the recently synthesized 312 MAX phase solid solutions in Ti-Zr-Al-C system [13].

Table 3
Mechanical properties of $(Ti_{1-x}Zr_x)_3SiC_2$ MAX phase obtained by nanoindentation, Vickers microindentation, ultrasonic pulse-echo method measurement and DFT calculations.

x (-)	Hardness (GPa)		Elastic modulus (GPa)		
	Nanoindentation	Vickers	Ultrasonic	Nanoindentation	Calculated
0	12.8 ± 1.0	2.8 ± 0.1	338.8 ± 10.7	255 ± 22	357
0.03	15.3 ± 0.5	4.2 ± 0.5	354.7 ± 8.7	266 ± 18	
0.06	14.9 ± 0.7	6.8 ± 0.2	341.9 ± 20	269 ± 17	
0.09	17.1 ± 0.5	7.3 ± 0.2	348.0 ± 13.5	282 ± 22	352
0.12	17.3 ± 1.0	8.3 ± 0.1	325.2 ± 5.7	278 ± 27	
0.17	16.3 ± 1.1	8.5 ± 0.2	338.4 ± 11.6	290 ± 24	
0.18					348
0.25					343

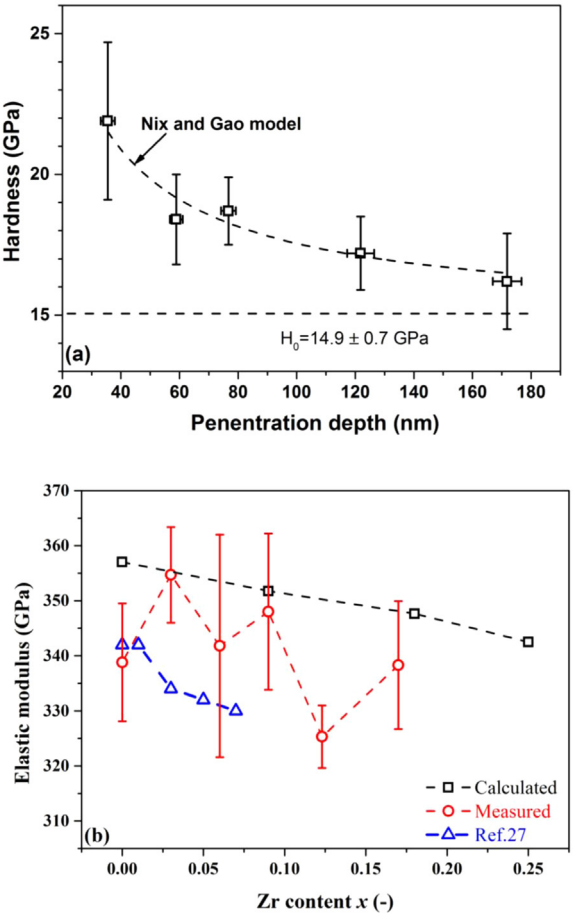

Fig. 7. The hardness and elastic modulus of the $(Ti_{1-x}Zr_x)_3SiC_2$MAX phase (a) hardness as a function of the indenter penetration depth for $(Ti_{0.94}Zr_{0.06})_3SiC_2$, (b) elastic modulus of $(Ti_{1-x}Zr_x)_3SiC_2$ obtained from ultrasonic pulse-echo measurements and DFT calculations as a function of Zr content.

Finally, the lattice parameter of $(Ti_{1-y}Zr_y)C$ solid solution by substitution of Ti with Zr (with a cubic rock salt crystal lattice) expanded from $a = 4.3192$ Å for $y = 0$ to $a = 4.3712$ Å for $y = 0.11$; see Table 2.

4.5. Hardness, elastic modulus and electronic structure of $(Ti_{1-x}Zr_x)_3SiC_2$ MAX phase solid solutions

The hardness by nanoindentation and the elastic modulus by ultrasonic measurement of the various $(Ti_{1-x}Zr_x)_3SiC_2$ synthesized under optimized conditions (cf. Table 3) are evaluated as function of their Zr content and the results are listed in Table 3. The nanoindetations were done within $(Ti_{1-x}Zr_x)_3SiC_2$ grains free of secondary phases. An example

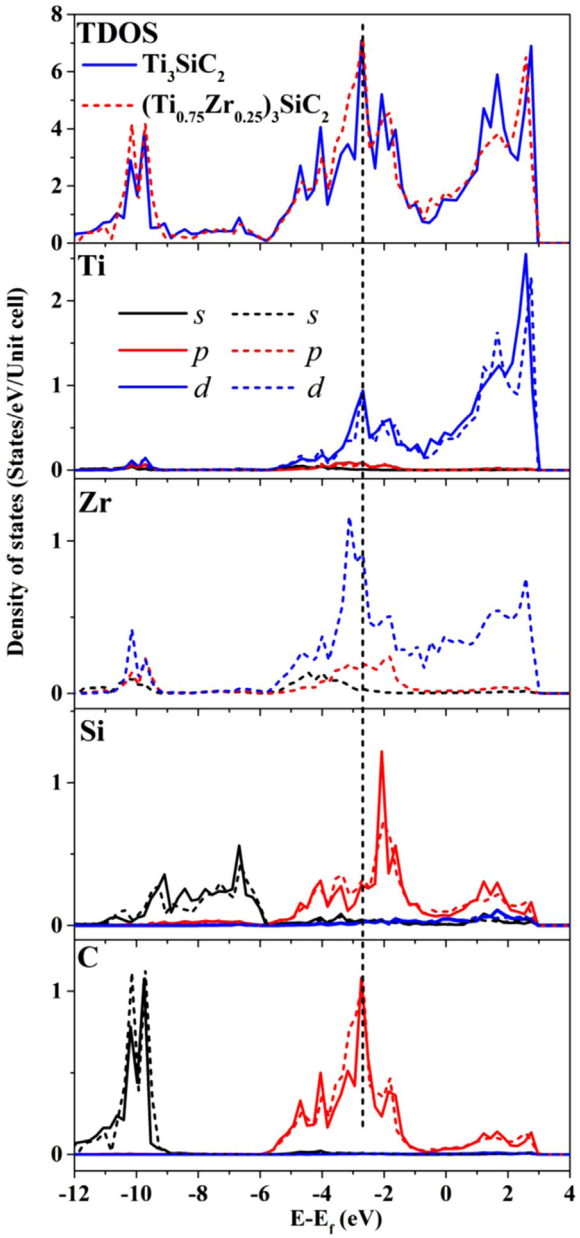

Fig. 8. Density of State (DOS) of $(Ti_{0.75}Zr_{0.25})_3SiC_2$MAX phase and partial DOS of Ti, Zr, Si and C atoms. Solid line: Ti_3SiC_2, Short dash line: $(Ti_{0.75}Zr_{0.25})_3SiC_2$MAX phase.

of the dependence of hardness on the penetration depth of the indenter is shown in Fig. 7(a). The hardness decreases with increasing

displacements and shows significant indentation size effect or load dependence. A similar indentation size effect has been observed for Ti_3SiC_2 [54], Ti_3SnC_2 [55] as well as Ti_3AlC_2 and related $Ti_3Al_{0.8}Sn_{0.2}C_2$ solid solutions [20]. Fitting the obtained hardness values to the Nix and Gao model [37] (see Fig. 7(a)), an intrinsic hardness of 14.9 ± 0.7 GPa is deduced for the $(Ti_{0.94}Zr_{0.06})_3SiC_2$ solid solution. The hardness of the other samples as a function of the Zr content is listed in Table 3. Within the Zr solid solution range of x in between 0 and 0.17, the hardness of $(Ti_{1-x}Zr_x)_3SiC_2$ increases with Zr content. The hardness of $(Ti_{1-x}Zr_x)_3SiC_2$ varied from 12.7 ± 1 GPa for Ti_3SiC_2 to 16.3 ± 1.1 GPa for $(Ti_{0.83}Zr_{0.17})_3SiC_2$, respectively; see Table 3. The hardness of the Ti_3SiC_2 obtained by nanoindentation is comparable with the values reported for Ti_3AlC_2 [20] and Ti_3SnC_2 [55].

The microhardness values of $(Ti_{1-x}Zr_x)_3SiC_2$ determined by Vickers hardness measurements shows a similar trend as the hardness values obtained from nanoindentations; see Table 3. The hardness increases with the amount of Zr added to the powder mixture due to an increasing amount of $(Ti_{1-y}Zr_y)C$ second phase in the sintered material; see Fig. 4. The microhardness values increased from 2.8 ± 0.1 GPa for Ti_3SiC_2 to 8.5 ± 0.2 GPa for $(Ti_{0.83}Zr_{0.17})_3SiC_2$. The lower hardness at high loads is attributed to the fact that at higher loads (i.e. larger contact area) multiple grains are involved in the deformation process. As a result, grain push-in and pull–out, or grain boundary de-cohesions takes place near the indents, leading to an underestimation of the actual nanohardness [20,55].

Our ab initio calculations predict that the elastic modulus values for $(Ti_{1-x}Zr_x)_3SiC_2$ solid solutions decrease only slightly from 357 to 342 GPa when the Zr content x changes from 0 to 0.25, as shown in Fig. 7(b) and listed in Table 3. The decrease in elastic modulus can be understood by considering the Total and Partial Density of States (TDOS and PDOS) of Ti_3SiC_2 and $(Ti_{0.75}Zr_{0.25})_3SiC_2$ MAX, which are depicted in Fig. 8. The TDOS of Ti_3SiC_2 at Fermi energy are mainly associated with the Ti-*d* electrons and there is almost no contribution of the C and Si electrons, which is in agreement with previous calculations [56,57]. Below the Fermi energy, distinct peaks can be observed at around − 2 eV and − 2.7 eV, indicating hybridization between Ti-*d* and Si-*p* and Ti-*d* and C-*p*, respectively. The partial substitution of Ti by Zr cause only minute changes in the DOS, e.g. the peak at around − 2.7 eV broadens due to hybridization between Zr-*d* and C-*p*. Hence, the observed similarity in the calculated elastic modulus upon Ti substitution by Zr can be rationalized by the rather similar electronic structures of Ti_3SiC_2 and $(Ti_{0.75}Zr_{0.25})_3SiC_2$. It is to be noted that the calculated elastic moduli applies to the ground-state, i.e. at 0 K, whereas the elastic modulus were measured at room temperature. The elastic modulus of a solid decreases with increasing temperature [58,59]. For example, the bulk modulus of Cr_2AlC decreases with 15% as the temperature goes from 0 to 1200 K [58]. Besides that, structural defects, such as porosity can have a prominent effect on the elastic modulus of the synthesized MAX phase [58,60]. However, for the Ti_3SiC_2 sample, a porosity of about 3% was determined, while the Zr containing samples exhibited a porosity of less than 1%. The presence of the second phases $(Ti_{1-y}Zr_y)C$ and Ti-Si-Zr intermetallics) having a higher elastic modulus (about 450 GPa) will, according to the rule of mixtures, increase the elastic modulus only 3% maximally.

The predicted elastic modulus values are in agreement with the reported elastic moduli of $(Ti_{1-x}Zr_x)_3SiC_2$ (x up to 0.07) solid solutions obtained by impulse excitation measurements [27] and the elastic modulus values (325–354 GPa) as obtained with ultrasonic measurements for the materials presented here; see Table 3. However, the elastic moduli of $(Ti_{1-x}Zr_x)_3SiC_2$ (x up to 0.17) solid solutions extracted from nanoindentation are 15 ~ 25% lower than the one obtained from ultrasonic measurements and ab initio calculations; see Table 3. The lower values of elastic moduli obtained from nanoindentation may be due effect of temperature [58,59] and porosity [58,60].

5. Conclusions

A series of almost pure $(Ti_{1-x}Zr_x)_3SiC_2$ MAX phase solid solutions with x varying between 0 and 0.17 were successfully synthesized by reactive Spark Plasma Sintering (SPS). $Ti_{1-y}Zr_yC$ and Ti-Si-Zr intermetallics were observed as a second phase. Their amounts increases with increasing amount of Zr added to the powder mixture, but decreased with increasing sintering temperature. It was not possible to synthesize Zr_3SiC_2. The lattice parameters of $(Ti_{1-x}Zr_x)_3SiC_2$ solid solutions with a hexagonal crystal lattice show an anisotropic lattice expansion as a function of the Zr content. The lattice parameter of the basal plane (i.e., along the a axis) increases more than the lattice parameter perpendicular to the basal plane (i.e., along the c axis). The dissolution of Zr into Ti_3SiC_2 has virtually no effect on its electronic structure and hence on its stiffness. The small reduction of the elastic modulus of $(Ti_{1-x}Zr_x)_3SiC_2$ from 357 to 342 GPa by increasing the Zr content form x is 0–0.25, can be understood based on concomitant, minute changes in electronic structure. The elastic moduli and lattice parameters of $(Ti_{1-x}Zr_x)_3SiC_2$ obtained from ab initio calculations are in excellent agreement with experimental observations. The hardness values of $(Ti_{1-x}Zr_x)_3SiC_2$ MAX phase solid solution as obtained from nanoindentation varied from 12.7 ± 1 GPa for Ti_3SiC_2 to 16.4 ± 1.1 GPa for $(Ti_{0.83}Zr_{0.17})_3SiC_2$ solid solution.

Acknowledgments

Financial support from German Research Foundation (Deutsche Forschungsgemeinschaft, DFG, SPP 1568 'Design and Generic Principles of Self-Healing Materials', SL184/1-2) and China Scholarship Council (CSC) for L. Qu (No. 201506680042) was appreciated. *Ab initio* calculations were performed with computing resources granted by JARA-HPC from RWTH Aachen University under project No. JARA0131.

References

[1] M.W. Barsoum, The $M_{N+1}AX_N$ phases: a new class of solids thermodynamically stable nanolaminates, Prog. Solid State Chem. 28 (2000) 201–281, https://doi.org/10.1016/S0079-6786(00)00006-6.
[2] M.W. Barsoum, M. Radovic, Elastic and mechanical properties of the MAX phases, Annu. Rev. Mater. Res. 41 (2011) 195–227, https://doi.org/10.1146/annurev-matsci-062910-100448.
[3] Z.M. Sun, Progress in research and development on MAX phases: a family of layered ternary compounds, Int. Mater. Rev. 56 (2011) 143–166, https://doi.org/10.1179/174 3280410Y.0000000001.
[4] S. Li, L. Xiao, G. Song, X. Wu, W.G. Sloof, S. Van Der Zwaag, Oxidation and crack healing behavior of a fine-grained Cr_2AlC ceramic, J. Am. Ceram. Soc. 96 (2013) 892–899, https://doi.org/10.1111/jace.12170.
[5] S. Li, G. Song, K. Kwakernaak, S. van der Zwaag, W.G. Sloof, Multiple crack healing of a Ti_2AlC ceramic, J. Eur. Ceram. Soc. 32 (2012) 1813–1820, https://doi.org/10.1016/j.jeurceramsoc.2012.01.017.
[6] S. Li, G. Bei, X. Chen, L. Zhang, Y. Zhou, M. Mačković, E. Spiecker, P. Greil, Crack healing induced electrical and mechanical properties recovery in a Ti_2SnC ceramic, J. Eur. Ceram. Soc. 36 (2016) 25–32, https://doi.org/10.1016/j.jeurcera msoc. 2015.09.019.
[7] P. Greil, Generic principles of crack-healing ceramics, J. Adv. Ceram. 1 (2012) 249–267, https://doi.org/10.1007/s40145-012-0020-2.
[8] Z. Sun, R. Ahuja, J.M. Schneider, Theoretical investigation of the solubility in $(M_xM'_{2-x})AlC$ (M and M′ = Ti, V and Cr), Phys. Rev. B: Condens. Matter 68 (2003), https://doi.org/10.1103/PhysRevB.68.224112 (224112.224111-224112.224114).
[9] S. Gupta, M.W. Barsoum, Synthesis and oxidation of V_2AlC and $(Ti_{0.5}, V_{0.5})_2AlC$ in air, J. Electrochem. Soc. 151 (2004) D24–D29, https://doi.org/10.1149/1.1639160.
[10] J.Y. Wang, Y.C. Zhou, Ab initio elastic stiffness of nano-laminate $(M_xM'_{2-x})AlC$(M and M′ = Ti, V and Cr) solid solution, J. Phys. Condens. Matter 16 (2004) 2819–2827, https://doi.org/10.1088/0953-8984/16/16/006.
[11] F.L. Meng, Y.C. Zhou, J.Y. Wang, Strengthening of Ti_2AlC by substituting Ti with V, Scr. Mater. 53 (2005) 1369–1372, https://doi.org/10.1016/j.scriptamat.2005.08.030.
[12] Y. Zhou, F. Meng, J. Zhang, New MAX-phase compounds in the V-Cr-Al-C system, J. Am. Ceram. Soc. 91 (2008) 1357–1360, https://doi.org/10.1111/j.1551-2916.2008.0 2279.x.
[13] B. Tunca, T. Lapauw, O.M. Karakulina, M. Batuk, T. Cabioc'h, J. Hadermann, R. Delville, K. Lambrinou, J. Vleugels, Synthesis of MAX phases in the Zr-Ti-Al-C system, Inorg. Chem. 56 (2017) 3489–3498, https://doi.org/10.1021/acs.inorgchem. 6b03057.

[14] P. Finkel, B. Seaman, K. Harrell, J. Palma, J.D. Hettinger, S.E. Lofland, A. Ganguly, M.W. Barsoum, Z. Sun, S. Li, R. Ahuja, Electronic, thermal, and elastic properties of $Ti_3Si_{1-x}Ge_xC_2$ solid solutions, Phys. Rev. B: Condens. Matter 70 (2004), https://doi.org/10.1103/PhysRevB.70.085104 (085104-085101-085104-085106).

[15] A. Ganguly, T. Zhen, M.W. Barsoum, Synthesis and mechanical properties of Ti_3GeC_2 and $Ti_3(Si_xGe_{1-x})C_2$ (x = 0.5, 0.75) solid solutions, J. Alloy. Compd. 376 (2004) 287–295, https://doi.org/10.1016/j.jallcom.2004.01.011.

[16] J.X. Chen, Y.C. Zhou, Effect of Si content on the oxidation resistance of $Ti_3Al_{1-x}Si_xC_2$ ($x \leq 0.25$) solid solutions at 1000–1400 °C in air, Oxid. Met. 65 (2006) 123–135, https://doi.org/10.1007/s11085-006-9007-0.

[17] J.X. Chen, Y.C. Zhou, J. Zhang, Abnormal thermal expansion and thermal stability of $Ti_3Al_{1-x}Si_xC_2$ solid solutions, Scr. Mater. 55 (2006) 675–678, https://doi.org/10.1016/j.scriptamat.2006.07.003.

[18] Y.C. Zhou, J.X. Chen, J.Y. Wang, Strengthening of Ti_3AlC_2 by incorporation of Si to form $Ti_3Al_{1-X}Si_xC_2$ solid solutions, Acta Mater. 54 (2006) 1317–1322, https://doi.org/10.1016/j.actamat.2005.10.057.

[19] G. Bei, B.J. Pedimonte, T. Fey, P. Greil, Oxidation behavior of MAX phase $Ti_2Al_{(1-x)}Sn_xC$ solid solution, J. Am. Ceram. Soc. 96 (2013) 1359–1362, https://doi.org/10.1111/jace.12358.

[20] G.P. Bei, V. Gauthier-Brunet, C. Tromas, S. Dubois, Synthesis, characterization, and intrinsic hardness of layered nanolaminate Ti_3AlC_2 and $Ti_3Al_{0.8}Sn_{0.2}C_2$ solid solution, J. Am. Ceram. Soc. 95 (2012) 102–107, https://doi.org/10.1111/j.1551-2916.2011.04846.x.

[21] S. Dubois, G.P. Bei, C. Tromas, V. Gauthier-Brunet, P. Gadaud, Synthesis, microstructure, and mechanical properties of $Ti_3Sn_{(1-x)}Al_xC_2$ MAX phase solid solutions, Int. J. Appl. Ceram. Technol. 7 (2010) 719–729, https://doi.org/10.1111/j.1744-7402.2010.02554. x.

[22] Z. Huang, H. Xu, H. Zhai, Y. Wang, Y. Zhou, Strengthening and tribological surface self-adaptability of Ti_3AlC_2 by incorporation of Sn to form $Ti_3Al(Sn)C_2$ solid solutions, Ceram. Int. 41 (2015) 3701–3709, https://doi.org/10.1016/j.ceramint.2014.11. 042.

[23] L. Cai, Z. Huang, W. Hu, C. Lei, S. Wo, X. Li, H. Zhai, Y. Zhou, Fabrication and microstructure of a new ternary solid solution of $Ti_3Al_{0.8}Si_{0.2}Sn_{0.2}C_2$ with high solid solution strengthening effect, Ceram. Int. 44 (2018) 9593–9600, https://doi.org/10.1016/j.ceramint. 2018.02.183.

[24] M.W. Barsoum, M. Ali, T. El-Raghy, Processing and characterization of Ti_2AlC, Ti_2AlN and $Ti_2AlC_{0.5}N_{0.5}$, Metall. Mater. Trans. A 31 (2000) 1857–1865, https://doi.org/10.1007/ s11661-006-0243-3.

[25] T. Cabioc'h, P. Eklund, V. Mauchamp, M. Jaouen, Structural investigation of substoichiometry and solid solution effects in $Ti_2Al(C_xN_{1-x})_y$ compounds, J. Eur. Ceram. Soc. 32 (2012) 1803–1811, https://doi.org/10.1016/j.jeurceramsoc.2011.12.011.

[26] G.P. Bei, B.J. Pedimonte, M. Pezoldt, J. Ast, T. Fey, M. Goeken, P. Greil, Crack healing in $Ti_2Al_{0.5}Sn_{0.5}C$–Al_2O_3 composites, J. Am. Ceram. Soc. 98 (2015) 1604–1610, https://doi.org/10.1111/jace.13496.

[27] W. De-Tian, H. Ling-Feng, Z. Li-Li, Z. Jie, B. Yi-Wang, Z. Yan-Chun, A new method to improve the high-temperature mechanical properties of Ti_3SiC_2 by substituting Ti with Zr, Hf, or Nb, J. Am. Ceram. Soc. 93 (2010) 1749–1753, https://doi.org/10.1111/j.1551-2916.2010.03637.x.

[28] T. Lapauw, D. Tytko, K. Vanmeensel, S. Huang, P.-P. Choi, D. Raabe, Ea.N. Caspi, O. Ozeri, M. to Baben, J.M. Schneider, K. Lambrinou, J. Vleugels, $(Nb_x, Zr_{1-x})_4AlC_3$ MAX phase solid solutions: processing, mechanical properties, and density functional theory calculations, Inorg. Chem. 55 (2016) 5445–5452, https://doi.org/10.1021/acs.inorgchem. 6b00484.

[29] M.W. Barsoum, T. El-Raghy, Synthesis and characterization of a remarkable ceramic: Ti_3SiC_2, J. Am. Ceram. Soc. 79 (1996) 1953–1956, https://doi.org/10.1111/ j.1151-2916. 1996.tb08018.x.

[30] H.B. Zhang, Y.W. Bao, Y.C. Zhou, Current status in layered ternary carbide Ti_3SiC_2, a review, J. Mater. Sci. Technol. 25 (2009) 1–38.

[31] A.B. 3962-15, Standard Test Methods for Density of Compacted Powder Metallurgy Products Using Archimedes' Principle, Standard, ASTM International, West Conshohocken, PA, USA, 2015.

[32] L. Lutterotti, S. Matthies, H.R. Wenk, MAUD: a friendly Java program for material analysis using diffraction, IUCr: Newsl. CPD 21 (1999) 14–15.

[33] David R. Black, Donald Windover, Albert Henins, J. Filliben, J.P. Cline, Standard reference material 660b for X-ray metrology, Adv. X-Ray Anal. 54 (2010) 140–148.

[34] S. Saunders, P. Karduck, W.G. Sloof, Certified reference materials for micro-analysis of carbon and nitrogen, Microchim. Acta 145 (2004) 209–213, https://doi.org/10.1007/s00604-003-0155-5.

[35] J. Woirgard, J.C. Dargenton, An alternative method for penetration depth determination in nanoindentation measurements, J. Mater. Res. 12 (1997) 2455–2458, https://doi.org/10.1557/JMR.1997.0324.

[36] W.C. Oliver, G.M. Pharr, An improved technique for determining hardness and elastic modulus using load and displacement sensing indentation experiments, J. Mater. Res. 7 (2011) 1564–1583, https://doi.org/10.1557/JMR.1992.1564.

[37] W.D. Nix, H. Gao, Indentation size effects in crystalline materials: a law for strain gradient plasticity, J. Mech. Phys. Solids 46 (1998) 411–425, https://doi.org/10.1016/ S00 22-5096(97)00086-0.

[38] S. Qu, Y. Huang, W.D. Nix, H. Jiang, F. Zhang, K.C. Hwang, Indenter tip radius effect on the Nix–Gao relation in micro- and nanoindentation hardness experiments, J. Mater. Res. 19 (2004) 3423–3434, https://doi.org/10.1557/JMR.2004.0441.

[39] J. Krautkrämer, H. Krautkrämer, Ultrasonic Testing of Materials, Springer Berlin Heidelberg, 1999.

[40] P. Hohenberg, W. Kohn, Inhomogeneous electron gas, Phys. Rev. 136 (1964) B864–B871, https://doi.org/10.1103/PhysRev.136.B864.

[41] G. Kresse, Ab initio molecular dynamics for liquid metals, J. Non-Cryst. Solids 192–193 (1995) 222–229, https://doi.org/10.1016/0022-3093(95)00355-X.

[42] G. Kresse, J. Hafner, Ab initio molecular-dynamics simulation of the liquid-metal-amorphous-semiconductor transition in germanium, Phys. Rev. B 49 (1994) 14251–14269, https://doi.org/10.1103/PhysRevB.49.14251.

[43] G. Kresse, D. Joubert, From ultrasoft pseudopotentials to the projector augmented-wave method, Phys. Rev. B 59 (1999) 1758–1775, https://doi.org/10.1103/PhysRevB. 59.1758.

[44] J.P. Perdew, K. Burke, M. Ernzerhof, Generalized gradient approximation made simple, Phys. Rev. Lett. 78 (1997), https://doi.org/10.1103/PhysRevLett.77. 3865 (1396-1396).

[45] P.E. Blöchl, O. Jepsen, O.K. Andersen, Improved tetrahedron method for Brillouin-zone integrations, Phys. Rev. B 49 (1994) 16223–16233, https://doi.org/10.1103/PhysRevB. 49.16223.

[46] H.J. Monkhorst, J.D. Pack, Special points for Brillouin-zone integrations, Phys. Rev. B 13 (1976) 5188–5192, https://doi.org/10.1103/PhysRevB.13.5188.

[47] F. Birch, Finite strain isotherm and velocities for single-crystal and polycrystalline NaCl at high pressures and 300°K, J. Geophys. Res. Solid Earth 83 (1978) 1257–1268, https://doi.org/10.1029/JB083iB03p01257.

[48] K. Wang, Foundations of Materials Engineering, Tsinghua University Press, Beijing, 2003.

[49] Y. Wang, A.H. Carim, Ternary phase equilibria in the Zr-Si-C system, J. Am. Ceram. Soc. 78 (1995) 662–666, https://doi.org/10.1111/j.1151-2916.1995.tb08229.x.

[50] C.E. Brukl, Ternary Phase Equilibria in Transition Metal-Boron-Carbon-Silicon Systems, Technical Report No. AFML TR-65–2, Part II, Air Force Materials Laboratory, Wright-Patterson Air Force Base, OH, 1966.

[51] H. Nowotny, B. Lux, H. Kudielka, Das Verhalten metallreicher, hochschmelzender Silizide gegenüber Bor, Kohlenstoff, Stickstoff und Sauerstoff, Mon. Chem. Verw. Teil. And. Wiss. 87 (1956) 447–470, https://doi.org/10.1007/BF00902640.

[52] B.H. Billings, D.E. Gray, American Institute of Physics Handbook, Third ed., McGraw-Hill, New York, 1972.

[53] K.T. Jacob, S. Raj, L. Rannesh, Vegard's law: a fundamental relation or an approximation? Int. J. Mater. Res. 98 (2007) 776–779, https://doi.org/10.3139/146.101545.

[54] B.J. Kooi, R.J. Poppen, N.J.M. Carvalho, J.T.M. De Hosson, M.W. Barsoum, Ti_3SiC_2: a damage tolerant ceramic studied with nano-indentations and transmission electron microscopy, Acta Mater. 51 (2003) 2859–2872, https://doi.org/10.1016/S1359-6454(03)00091-0.

[55] C. Tromas, N. Ouabadi, V. Gauthier-Brunet, M. Jaouen, S. Dubois, Mechanical properties of nanolaminate Ti_3SnC_2 carbide determined by nanohardness cartography, J. Am. Ceram. Soc. 93 (2010) 330–333, https://doi.org/10.1111/j.1551-2916.2009.03412.x.

[56] J.-Y. Wang, Y.-C. Zhou, Polymorphism of Ti_3SiC_2 ceramic: first-principles investigations, Phys. Rev. B 69 (2004) 144108, https://doi.org/10.1103/PhysRevB.69. 144108.

[57] Y. Bai, X. He, Y. Sun, C. Zhu, M. Li, L. Shi, Chemical bonding and elastic properties of Ti_3AC_2 phases (A = Si, Ge, and Sn): a first-principle study, Solid State Sci. 12 (2010) 1220–1225, https://doi.org/10.1016/j.solidstatesciences.2010.03.007.

[58] J.M. Schneider, D.P. Sigumonrong, D. Music, C. Walter, J. Emmerlich, R. Iskandar, J. Mayer, Elastic properties of Cr_2AlC thin films probed by nanoindentation and ab initio molecular dynamics, Scr. Mater. 57 (2007) 1137–1140, https://doi.org/10.1016/j.scrip tamat.2007.08.006.

[59] B. Manoun, R.P. Gulve, S.K. Saxena, S. Gupta, M.W. Barsoum, C.S. Zha, Compression behavior of M_2AlC (M = Ti, V, Cr, Nb, and Ta) phases to above 50 GPa, Phys. Rev. B 73 (2006) 024110, https://doi.org/10.1103/PhysRevB.73.024110.

[60] M.M.M. Carrijo, H. Lorenz, I. Filbert-Demut, G.M. de Oliveira Barra, D. Hotza, X. Yin, P. Greil, N. Travitzky, Fabrication of Ti_3SiC_2-based composites via three-dimensional printing: influence of processing on the final properties, Ceram. Int. 42 (2016) 9557–9564, https://doi.org/10.1016/j.ceramint.2016.03.036.